Photoacid−Base Reaction in Ice via a Mobile L-Defect

Anna Uritski and Dan Huppert*

Raymond and Beverly Sackler Faculty of Exact Sciences, School of Chemistry, Tel Aviv University, Tel Aviv 69978, Israel

Received: August 28, 2007; In Final Form: December 19, 2007

A time-resolved emission technique was employed to study the photoprotolytic cycle of two photoacids 2-naphtol-6-sulfonate (2N6S) and 2-naphtol-6,8-disulfonate (2N68DS) in ice in the presence of a low concentration of a weak base fluoride ion. We found that an additional proton-transfer process occurs in ice doped with F^- ions. This reaction takes place between a mobile L-defect (created by static F^- ions) and the photoacid. We used a diffusion assisted reaction model, based on the Debye−Smoluchowski equation, to account for the direct reaction of the L-defect with the excited photoacid.

Introduction

Excited-state proton transfer (ESPT) from a photoacid is used as a common tool to study various aspects of proton-transfer reactions.[1−3,4−11] In previous studies we used photoacids to transfer protons to the ice lattice.[12−14] The photoprotolytic cycle of a photoacid in liquid and in ice includes two steps: a reactive step followed by a diffusive step.[17] In the reactive step a proton is transferred from a photoacid to a solvent molecule. The proton then diffuses in the liquid solvent or in ice. The deprotonated photoacid can recombine geminately with the diffusing proton and repopulates the protonated form of the photoacid. The photoprotolytic cycle can be easily monitored by time-resolved emission techniques. The diffusing proton can monitor the microscopic environment surrounding the excited photoacid molecule.

Water and ice are important and unique materials on our planet. If liquid water is frozen under normal atmospheric conditions it forms a crystalline solid with hexagonal symmetry which is referred to as *hexagonal ice*. The physics of ice was extensively studied over many centuries. The properties of ice were summarized in several books.[15−18] Many of the electrical properties of ice are unusual and, as a result, they were the subject of intensive experimental and theoretical investigations for many decades. Ice exhibits a high static relative permittivity which is comparable to that of liquid water. Ice also provides a good example of electrical conduction by transfer of protons which have mobilities of about the same order of magnitude as liquid water. Approximately at the freezing point, the conductance[19] of ice is relatively large; however, it drops rapidly as the temperature decreases. The theory of Jaccard[20] is used to explain the electrical conduction and the dielectric properties of ice. According to Jaccard's theory, the electrical properties of ice are largely due to two types of defects within the crystal structure. (1) Ion defects are produced when a proton moves from one end of the bond to the other, thus creating a H_3O^+, OH^- ion pair. Conduction is then possible by means of successive proton jumps. (2) Bjerrum defects[21] are orientational defects caused by the rotation of a water molecule to produce either a doubly occupied bond (D-defect) or a bond with no protons (L-defect). The mechanism of excess proton transfer in ice was investigated by Ohmine and co-workers[22] using the QM/MM method. By analyzing the potential surface, the normal modes, and the interaction between the excess proton and the defects, they proposed that the excess proton is localized in an L-defect in ice. Podeszwa and Buch[23] studied the structure and dynamics of orientational defects in ice by molecular dynamics simulation. They found the defect structure to be quite different from the one originally proposed by Bjerrum.[21] Two basic structures were identified for the D-defect and one dominant structure was obtained for the L-defect. Typically, one water molecule in an L-defect is displaced ≈1 Å from the crystal lattice site. Defect jumps occur via vibrational phase coincidence.

Many hydrophobic and hydrophilic compounds get excluded when water is frozen. For example, when NaCl solution is frozen the chloride ion gets incorporated in ice but the rejected sodium cations stay in quasi-liquid layer at the grain boundaries or at the solution.[24,25] In the solid phase, the dopants, like the organic photoacids, tend to expel from the crystallites to the grain boundaries and, as a consequence, the luminescence intensity in frozen samples is strongly reduced. The net result is an unreliable time-resolved emission measurement in the ice-phase of both acid (ROH*) and base (RO^-*) forms. The problem of incorporation of the photoacid into the ice-phase was unnoticed when a small amount of methanol of ∼1% mole fraction was added to the solution.

In this study we explore the effect of methanol concentration in ice on the photoprotolytic cycle of a photoacid. The main findings are that at a sufficiently low concentration of methanol 0.25−1% (of mole fraction) the change in the proton-transfer rate is only by about 10% in the temperature range 200−270 K. At larger methanol concentration, more than 5% (mole fraction), the proton-transfer rate in methanol-doped ice strongly decreases as a function of the mole fraction of methanol.

The main part of the present work is devoted to the study of the photoprotolytic cycle in methanol-doped ice in the presence of a small concentration of a mild base, the fluoride ion. For this purpose we used two photoacids, 2-naphtol-6-sulfonate (2N6S) and 2-naphtol-6,8-disulfonate (2N68DS). 2N6S is a weak photoacid pK* ∼ 2.0 whereas 2N68DS is a strong photoacid pK* ∼ 0.7. At room temperature the proton-transfer

* Corresponding author: Dan Huppert. E-mail: huppert@tulip.tau.ac.il. Telephone: 972-3-6407012. Fax: 972-3-6407491.

10.1021/jp076874q CCC: $40.75
Published on Web 03/20/2008

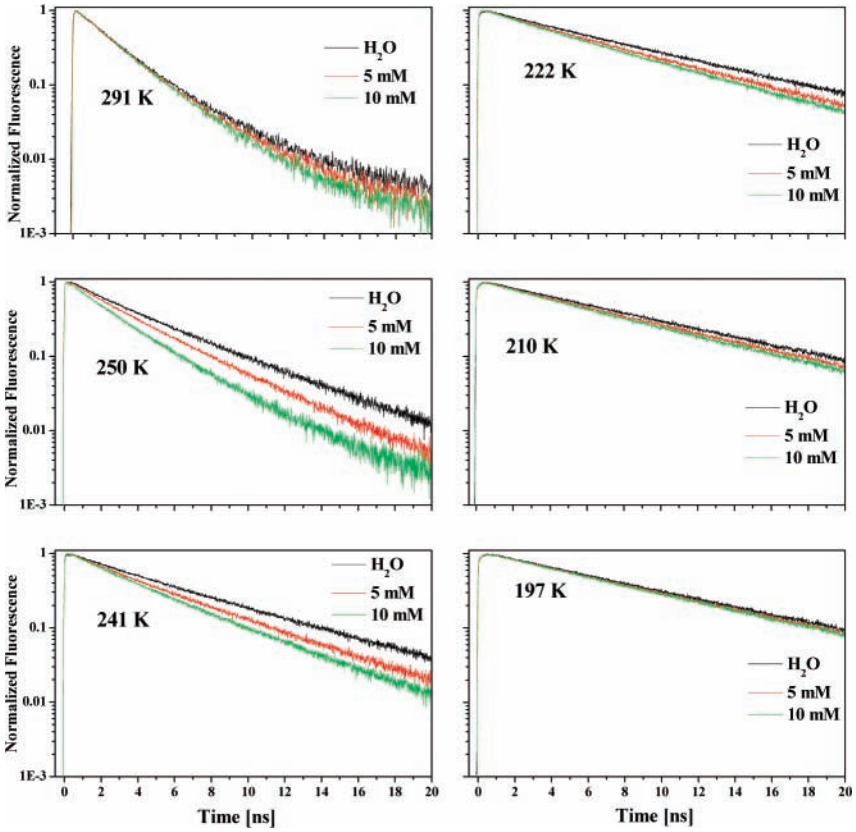

Figure 1. Time-resolved emission of ROH of 2N6S, measured at 360 nm in 5 and 10 mM of KF methanol-doped ice at different temperatures.

time constant of these photoacids in the excited-state is 800 and 50 ps for 2N6S and 2N68DS respectively. In fluoride doped ice we found that the rate of proton transfer increases in both photoacids in the temperature range 200−270 K.

Experimental Section

We used the time-correlated single-photon counting (TCSPC) technique to measure the time-resolved emission of the photoacids. For sample excitations, we used a cavity dumped Ti:sapphire femtosecond laser, Mira, Coherent, which provides short, 80 fs, pulses. The laser harmonics SHG and THG (third harmonic generation) operate over the spectral range of 380−400 nm, and for THG 260−290 nm. The cavity dumper operates with the relatively low repetition rate of 500 kHz. The TCSPC detection system is based on a Hamamatsu 3809U, photomultiplier and Edinburgh Instruments TCC 900 computer module for TCSPC. The overall instrumental response was about 35 ps (fwhm). The excitation pulse energy was reduced to about 10 pJ by neutral density filters.

The 2N6S and 2N68DS of analytical grade were purchased from Kodak. Potassium fluoride was purchased from Fluka. For transient measurements the sample concentrations were between 2×10^{-4} and 2×10^{-5} M. Deionized water had a resistance of >10 MΩ. Methanol, of analytical grade, was purchased from Fluka. All chemicals were used without further purification. The solution pH was about 6.

The temperature of the irradiated sample was controlled by placing the sample in a liquid N_2 cryostat with a thermal stability of approximately ± 1.5 K.

Ice samples were prepared by first placing the cryogenic sample cell for about 20 min at a temperature of about 273 K. The second step involved a relatively rapid cooling (10 min) to a temperature of about 250 K. Subsequently, the sample freezes within 5 min. To ensure ice equilibration, prior to the time-resolved measurements, the sample temperature was kept for another 30 min at about 250 K.

Results

Time-Resolved Emission. Figure 1 shows the time-resolved emission acquired by a time-correlated single photon counting technique of ROH the protonated form of 2N6S, of three samples at various temperatures in the region of 200 K < T < 300 K. The first sample contains the photoacid in ice doped with 1% (mole fraction) methanol in the absence of fluoride ion, while the second and third samples also contain 5 and 10 mM KF respectively. The samples were excited by 270 nm 250 fs pulses (THG of a mode locked cavity dumped Ti:sapphire laser) at a repetition rate of 500 kHz. As seen in the figure, for a particular temperature the fluorescence decay curves of the samples containing 5 and 10 mM KF differs from the sample without it. The long time nonexponential tail is strongly reduced in samples containing 5 and 10 mM KF. We explain this phenomenon by the efficient reaction of the mobile proton in ice with the static F^- surrounding the excited photoacid molecule, or by the mobile L-defect created by an F^- ion (L-defect properties are described in the discussion section). The average distance of an F^- ion from an excited photoacid (very small concentration) is about half of the average distance between the F^- ions, which is 55 Å for a 10 mM solution. Thus, the proton scavenging reaction takes place at an average distance of about 10 water molecules from the photoacid itself (the O−O distance in hexagonal ice is ∼ 2.75 Å). The time-resolved data can be fit by the reversible-geminate recombination model with the inclusion of a proton scavenger in solution,[26] (see the discussion section for a brief description of this model).

In addition to the reduced long-time fluorescence tail, one can easily observe that in ice the initial fast and nearly exponential decay rate is also enhanced in the presence of 5

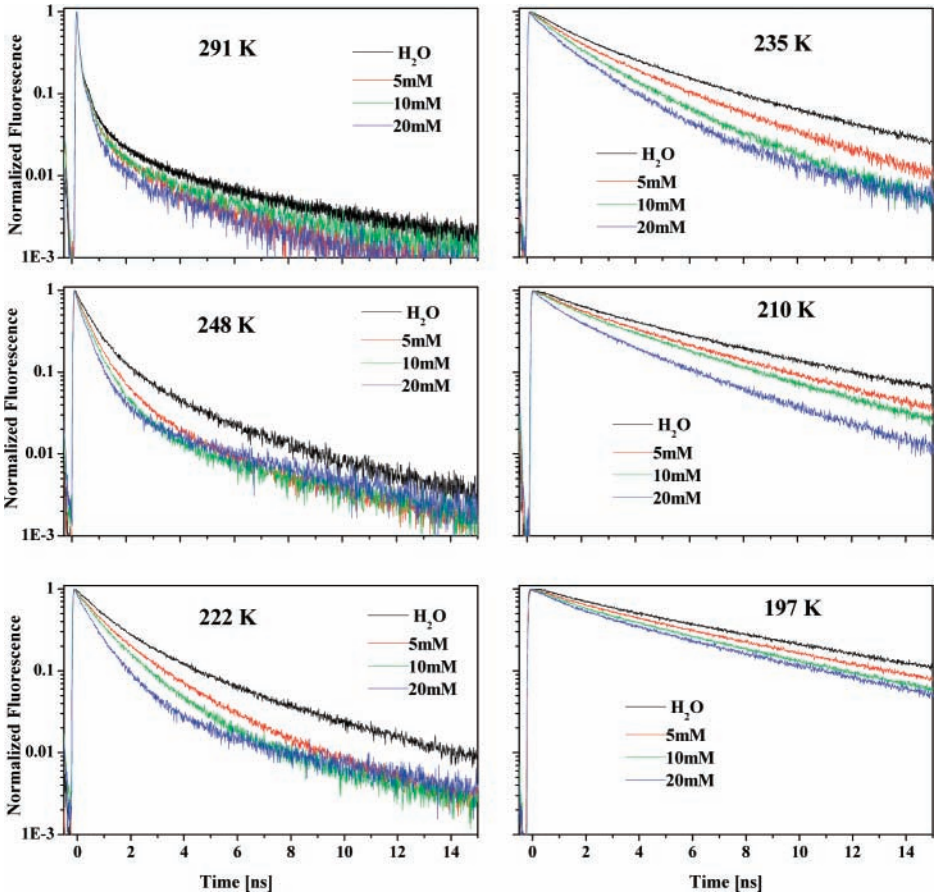

Figure 2. Time-resolved emission of ROH of 2N68DS, measured at 380 nm in 5, 10, and 20 mM of KF methanol-doped ice at different temperatures.

and 10 mM KF. In liquid water at room temperature the proton-transfer rate constant of 2N6S is $k_{PT} \equiv 1.2$ ns^{-1}, and thus the proton is transferred with a time constant of about 800 ps. In previous studies,[27] we found the proton-transfer rate constant in ice at about 268 K is smaller by a factor of approximately 2.5, $k_{PT} \equiv 0.5$ ns^{-1}. The temperature dependence of k_{PT} of 2N6S and other photoacids in ice is quite complex. In the high-temperature region of 240 K $< T <$ 270 K, the temperature dependence of k_{PT} is large, but not constant. At about 245 K, the value of k_{PT} of 2N6S $\sim$ 0.1 ns^{-1} and is about the same as the radiative rate constant ($\tau_{rad} \approx 8$ ns). A simple relation connects the relative fluorescence intensities of the two bands with the excited-state proton-transfer rate, and the radiative rates are given by

$$\phi'/\phi = \frac{k_{PT}}{k_{rad}} \tag{1}$$

where ϕ and ϕ' are the fluorescence quantum yields of the protonated and deprotonated forms of the photoacid respectively. k_{PT} and k_{rad} are the rate constants for the proton transfer and for the radiative process respectively. Thus, the efficiency of the photoprotolytic process strongly reduces at low temperature when $k_{PT} < k_{rad}$. At 220 K $< T <$ 270 K in ice containing 10 mM KF the rate of proton transfer from 2N6S is much larger than in ice samples in the absence of KF. Below 210 K the proton-transfer rate to the solvent and the direct proton transfer to an L-defect are much smaller than the radiative rate and hence both proton transfers cannot be observed by a time-resolved emission technique (see Figure 1).

Figure 2 shows the time-resolved emission of ROH in the protonated form of 2N68DS of four samples at various temperatures in the temperature region of 180 K $< T <$ 300 K. One of the samples does not contain KF whereas the other samples contain 5, 10, and 20 mM KF. In the liquid state the presence of small concentrations of KF affects only the ROH fluorescence long-time tail that arises from the geminate recombination process. The proton is first transferred from the photoacid to the solvent. The diffusing proton in solution is subsequently trapped by the reaction

$$H_3O^+ + F^- \rightarrow HF + H_2O \tag{2}$$

In liquid the proton transfer to the solvent is a fast process and the direct proton-transfer process can be detected only at large KF concentrations of $c \geq 0.25$ M

$$F^- + ROH^{-*} \rightarrow HF + RO^{-*} \tag{3}$$

The direct reaction shortens the early decay-time of the ROH time-resolved emission signal. The overall decay time, τ_{eff}, is given by

$$1/\tau_{eff} = k_{PT} + k_R + k_{rad} \tag{4}$$

where k_R is the direct reaction of the proton transfer to the fluoride. In the liquid state at an F^- base concentration of 10 mM the direct proton transfer is not observed.

Figure 3 shows the time-resolved emission of the RO^- band of 2N6S of three samples at several temperatures measured at 440 nm about the peak position of the RO^- emission band. The samples are slightly acidic and the excitation wavelength is at 270 nm, within the ROH absorption band. The first ice sample does not contain KF, whereas the second and third samples also contain 5 and 10 mM KF. The liquid samples at 290 K and the

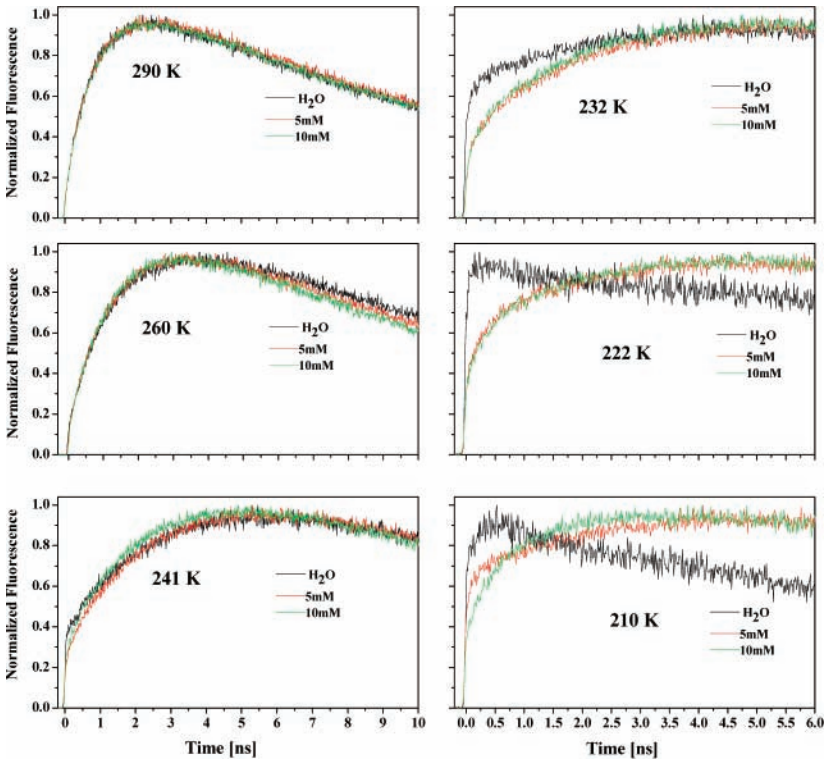

Figure 3. Time-resolved emission of RO^- of 2N6S, measured at 440 nm in 5 and 10 mM of KF methanol doped at different temperatures.

ice samples at 260 K show a rise-time followed by an exponential decay with a lifetime of about 12 ns, corresponding to the excited-state lifetime of the RO^- form. The rise-time of the RO^- emission signal fits the decay time of the ROH form. In the liquid the rise-time is determined by the ESPT to the solvent and by the ROH excited-state lifetime. In the solid the rise-time rate is also determined by the reaction between the mobile L-defect and the photoacid. At 290 K (liquid) and 260 K (ice) the relatively small difference between the effective decay time of the ROH in the absence and in the presence of KF is not large enough to affect the rise-time of the RO^-. At a temperature of 241 K the rise-time of the samples containing KF is faster than the one of the samples in the absence of KF. It is also noticed that the signal of the "pure" sample exhibits a large fast component of relative amplitude of about 0.35, whereas the signals of the samples containing KF show much smaller amplitudes of about 0.22 than of the fast component. The fast component arises from the contribution of the ROH band due to the overlap of the two bands (the ROH and the RO^-) at 440 nm (the peak of the RO^- band). In the case of a low temperature, where $k_{PT} < k_r$, the relative amplitude of the fast component increases in the signal measured at the RO^- peak. In the extreme case of a very low temperature where $k_{PT} \ll k_r$, the signal only consists of the contribution of the ROH. The decay time of the ROH signal at a temperature below 230 K is about that of the excited-state lifetime $\tau \sim 8$ ns. Signals measured at low temperatures of 210, 222, and 232 K show that the direct proton transfer from the photoacid to the solvent is very slow and hence the process is inefficient within the excited-state lifetime. The steady-state emission of a pure sample consists only of the ROH band. The time-resolved signal of a pure sample at 440 nm consists of a fast rise-time followed by an exponential decay time of about 8 ns ($\tau_{rad}^{ROH} = 8$ ns) rather than 12 ns ($\tau_{rad}^{RO-} = 12$ ns) in the samples containing KF. In contrast to the signal shape of a pure sample the signals of samples containing KF show a rise-time that depends on the KF concentration. At these low temperatures the steady-state emission of samples containing KF consists of two emission bands, that of ROH and that of RO^-.

Figure 4 shows the time-resolved emission of the RO^- band of 2N68DS at several temperatures measured at 470 nm close to the RO^- emission peak. The signals of samples contain 5, 10, and 20 mM of KF are compared with that of a sample without KF. As seen in the figure the rise-time of the fluorescence signal depends on the KF concentration. This result fits nicely the faster decay rate of the ROH band in the presence of KF in methanol-doped ice.

The Effect of Methanol. Figure 5 shows the effect of methanol concentration on the time-resolved emission signal of the ROH of 2N68DS in methanol-doped H_2O ice. As seen in the figure the effect of methanol concentration in the low methanol concentration range of 0.25−1% mole fraction is not large at all temperatures including the liquid state. As the methanol concentration gets smaller the proton rate becomes larger. The difference in the rate constant that is determined from the initial slope is not large, and is of the order of about 10%.

Figure 6 shows the effect of methanol concentration on the time-resolved emission of the ROH of 2N68DS in methanol-doped H_2O ice in the presence of 5 mM KF. In the liquid state, at the short times the decay curves of the ROH are almost unaffected by the presence of KF. In ice in the presence of KF the effect of methanol concentration on the short time decay rate of the ROH signal is large, much larger than in the absence of KF. As the methanol concentration gets larger the change in the decay rate of the ROH signal between samples with and without KF becomes smaller. This effect is qualitatively explained as follows. The mobile L-defect created by the weak base, the F^- anion, reacts with methanol to form a localized L-defect attached to a methanol molecule.

Figure 7 shows the time-resolved emission of the ROH band in methanol-doped ice at various methanol concentrations of two samples; that of 2N68DS in the presence of 5 mM KF and for comparison a sample in which KF is absent. The comparison

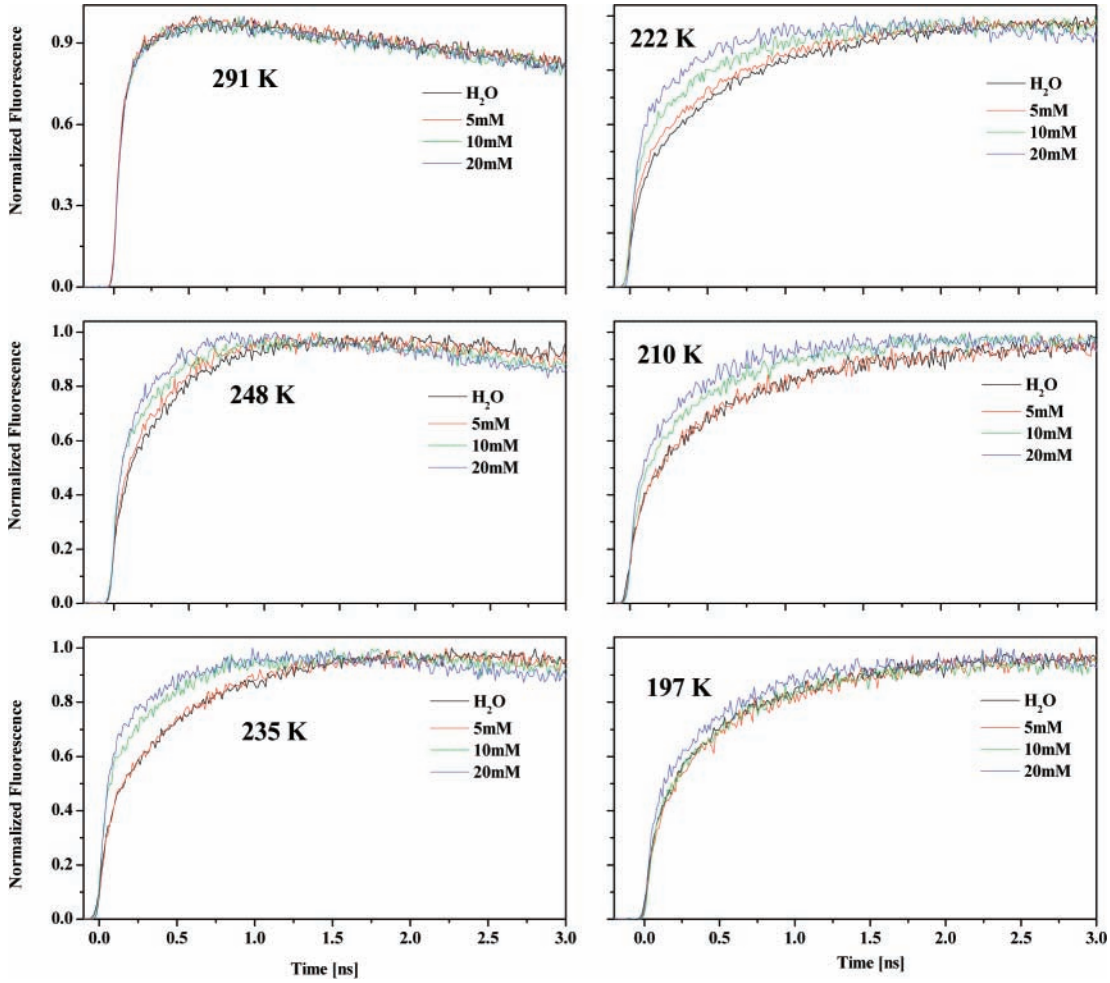

Figure 4. Time-resolved emission of RO^- of 2N68DS, measured at 470 nm in 5, 10, and 20 mM of KF in methanol-doped ice at different temperatures.

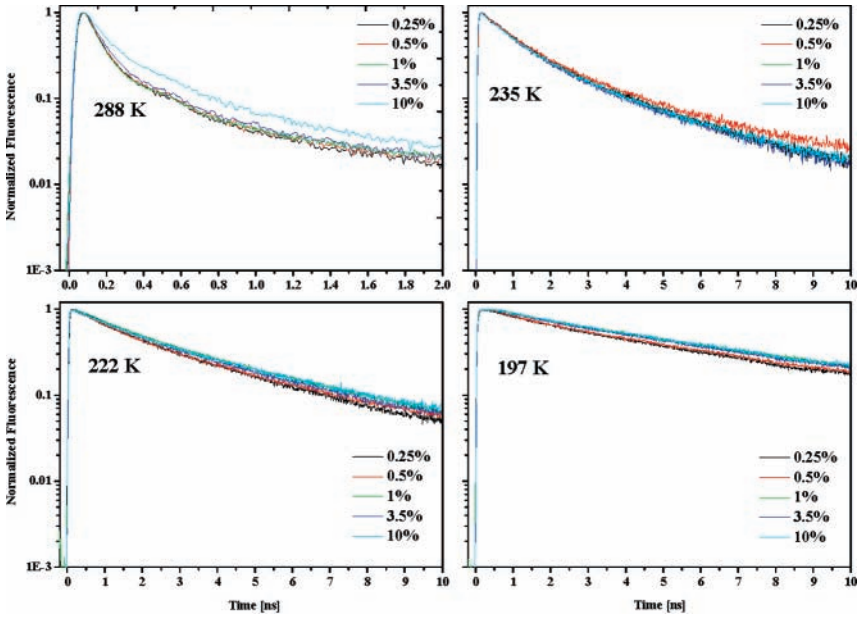

Figure 5. Time-resolved emission of the ROH band of 2N68DS in methanol-doped ice sample of various methanol concentrations.

between the two decay curves enables to observe the effect of methanol concentration on the direct proton-transfer reaction between the mobile L-defect and the excited ROH form of the photoacid. The smaller the methanol concentration the larger the effective reaction rate of the mobile L-defect with ROH. In the extreme case of large methanol concentration (3.5% and 10%) the emission decay curves of the ROH in the ice phase (at all temperatures studied) of samples with and without KF are almost identical. The results of the high methanol concentration samples indicate that L-defects are either trapped in these samples or the local methanol concentration surrounding the photoacid is large and therefore prevents the proton-transfer

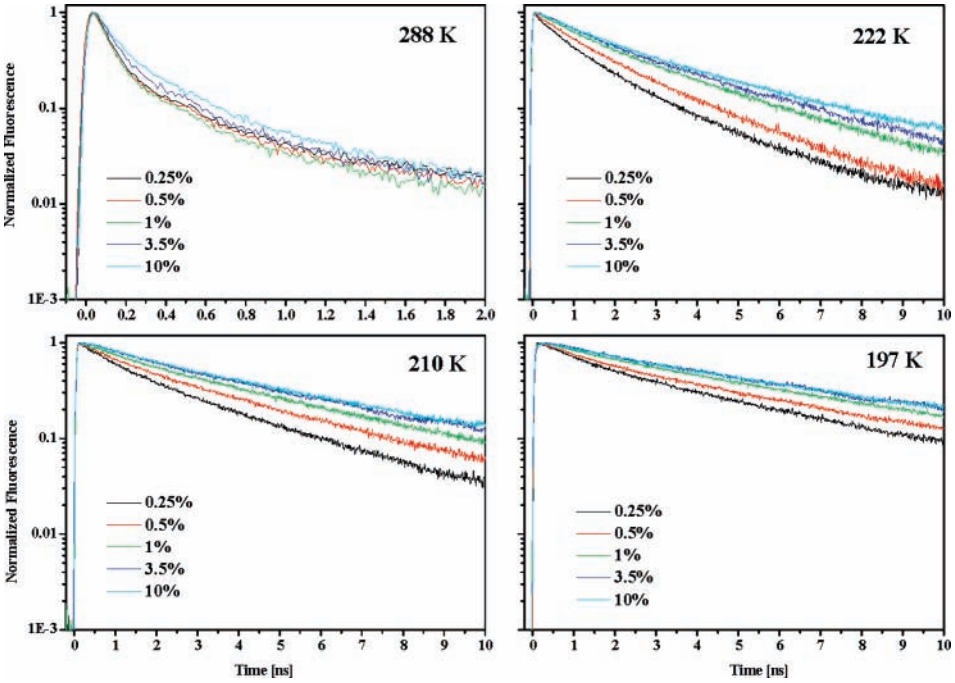

Figure 6. Time-resolved emission of the ROH band of 2N68DS in methanol-doped ice of various methanol concentrations in the presence of 5 mM KF (see text).

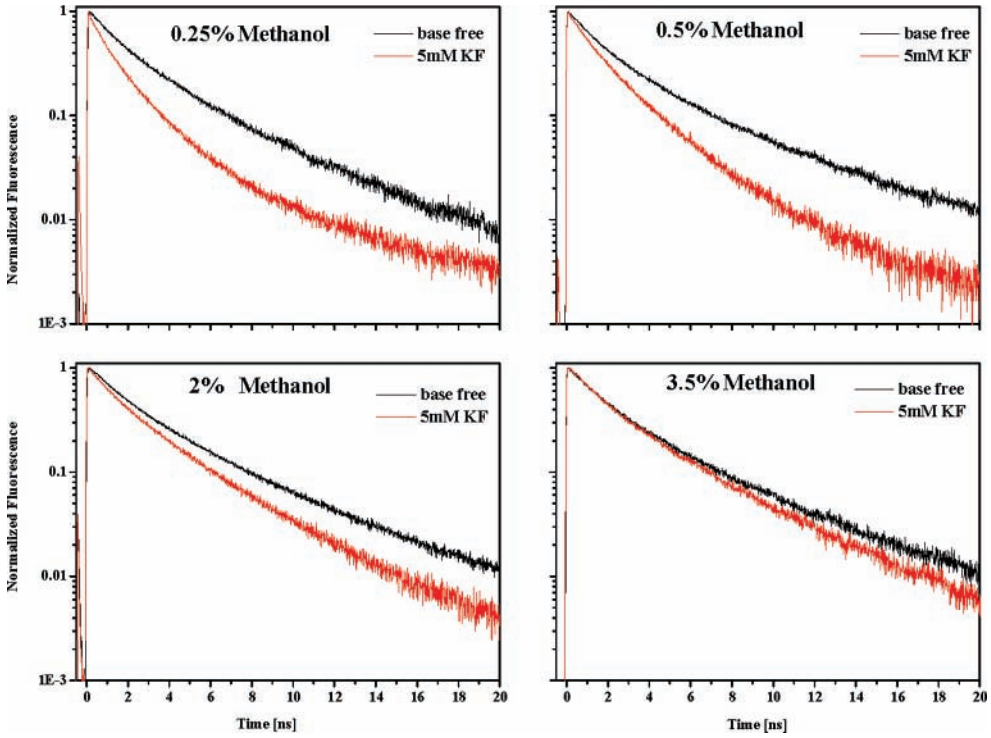

Figure 7. Time-resolved emission of the ROH band of 2N68DS in methanol-doped ice of samples at 222 K of various methanol concentrations. The upper curve in each panel is of a pure sample, whereas the lower curve is of a sample that contains 5 mM KF. Note that at large methanol concentrations, the two decay curves are almost identical.

process from the photoacid to the L-defect. In pure methanol liquid solution at room temperature the excited-state proton-transfer rate to the methanol solvent is very small. From time-resolved and the steady-state data we estimate that the rate is about 10 times slower than the radiative rate $k_{rad} = 0.12$ ns^{-1}, i.e. about 1000 times smaller than in pure water. Thus, if the photoacid is completely surrounded by methanol, both proton-transfer reactions are prevented.

Characterization of the Position and Average Distances of Photoacid Molecules in Polycrystalline Ice Samples. Pure ice is known to be a bad solvent.[18] It occurs that upon controlled slow freezing most of the dopants are extracted out of the crystal and therefore concentrates at the grain boundary. In our initial experiments on the photoprotolytic cycle of the photoacid in pure ice,[12−14] we noticed that the frozen samples are nonfluorescent, while for the liquid samples the fluorescence is at least 3 orders of magnitude more intense. We explained the lack of fluorescence of the photoacid in "pure" ice samples by the aggregation of the photoacid molecules at the grain boundary. Dimerization of two photoacid molecules causes the annihilation

of the overall transition dipole moment which will lead to the reduction of the fluorescence intensity. We found a procedure to overcome the aggregation of the photoacid molecules upon sample freezing. To prevent the aggregation we added to a pure aqueous solution 1% of methanol (by mole ratio). The methanol probably serves as a mediator between the hydrophobic aromatic rings of the photoacid with the ice water molecules. In numerous experiments we found that the fluorescence intensity of the frozen methanol-doped ice sample containing the photoacid is "behaving properly".

Here we list a set of spectroscopic parameters of several photoacids in methanol-doped ice that indicate that the photoacid molecules are indeed in the bulk of the polycrystalline sample and not at the grain boundaries:

1. The time integrated fluorescence intensities (the steady-state spectra) of both ROH and RO^- bands of the photoacid are about the same as for the liquid-state samples.

2. The spectroscopic structures of the steady-state emission of the ROH and RO^- bands in ice are similar to the liquid state except for (as expected) a small blue shift and a smaller bandwidth (these parameters are temperature dependent). When both the methanol and the photoacid are excluded while water is frozen, the methanol provides a uniform solvation surface region and the spectroscopic data of the photoacid are expected to be more like those of a photoacid in bulk methanol, rather than those of water. In a methanol solution the proton-transfer rate is slower than in pure water by a factor of about 1000. The width and position of the ROH and RO^- bands strongly depend on the solvent. In methanol the RO^- band is blue-shifted by about 500 cm^{-1} and the width decreases by about 300 cm^{-1}. This is clearly not the case based on the spectroscopic properties of a photoacid in frozen methanol-doped ice samples.

3. The repeatability and the reproducibility of the steady-state emission spectra as a function of temperature are excellent, as was measured by us for several hundred samples.

4. Time-resolved emission measured by the time correlated single photon counting technique of photoacids in methanol-doped ice at a large temperature range is exactly reproducible with all the fine details of the complex decay pattern along many orders of magnitude.

5. X-ray diffraction of a methanol-doped frozen water samples (270−100 K) shows a polycrystalline diffraction pattern.

Determination of the Average Distance of the Photoacid Molecules in Polycrystalline Methanol-Doped Ice Samples. We performed electronic energy transfer experiments to better characterize the position of the photoacid in the methanol-doped samples. Electronic energy transfer (EET) is a well studied photophysical process, involving dipolar interactions between two chromophores. Förster showed[28] that the energy transfer rate, k_{ET}, has the following form

$$k_{ET} = \frac{1}{\tau_D} + \frac{{R_0}^6}{r^6 \tau_D} \tag{5}$$

$${R_0}^6 = \frac{9000(\ln 10)\kappa^2}{128\pi^5 n^4 N_A} J \tag{6}$$

$$J = \int_0^\infty f(\lambda)\epsilon(\lambda)\lambda^4 \, d\lambda \tag{7}$$

where r is the donor−acceptor distance, τ_D is the spontaneous emission lifetime of the donor, n is the refractive index of the medium between the donor and acceptor, N_A is Avogadro's number, κ^2 is the orientational factor, and J is the normalized

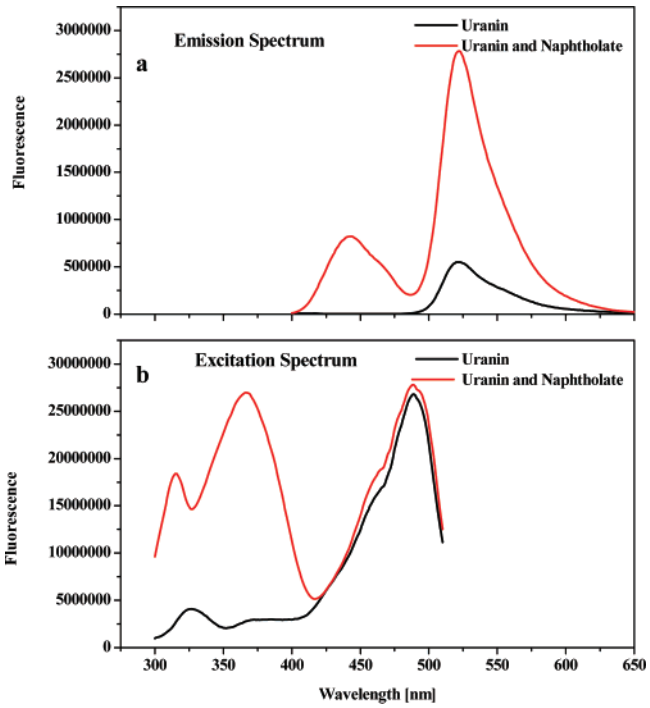

Figure 8. (a) Steady-state emission spectrum of two samples: uranin in water and a mixture of donor (2N68DS) and acceptor (uranin). (b) Excitation spectra of the same solutions as in part a.

spectral overlap integral. The time dependence of the excited-state population of the donor surrounded by a homogeneous distribution of acceptors in a bulk material like liquid solution and possibly bulk ice is given by

$$\rho(t) = \exp[-\tau_D - g4/3\pi^{3/2} n_A {R_0}^3 (t/\tau_D)^{1/2}] \tag{8}$$

where n_A is the number density of the acceptor, $g = (3/2\langle\kappa^2\rangle)^{1/2}$, $\langle\kappa^2\rangle$ is an averaged orientation factor usually taken as $\langle\kappa^2\rangle = 2/3$.

When the photoacid molecules are at grain boundary and not in the bulk, the average distance between adjacent molecules is much smaller than in the case when the same amount of photoacid molecules are homogeneously distributed within the microcrystals. The Förster electronic energy transfer process[28] is very sensitive to the distances between the donor and the acceptor and may be used to characterize the distances between molecules in frozen samples. We calculated the average distance between molecules for a sample that forms cubic microcrystals of the size of 10 μm and a concentration of photoacids of 1 mM. The bulk average distance is about 100 Å while at the grain boundary the average distance between photoacid molecules is about 5 Å. Thus the EET process for the two extreme cases of the position of the photoacid in the ice sample described above should show large differences.

The experiments described below indicate that the donor−acceptor distances in liquid aqueous solution are also preserved in the polycrystalline ice samples. Figure 8a shows the steady-state emission of two samples in aqueous solution; a sample that contains only the acceptor and a solution that contains both the donor and the acceptor at the same concentrations as the separated samples at room temperature. The donor in the EET experiments is a photoacid, 2-naphtol-6,8-disulfonate (2N68DS) in its deprotonated form RO^-. The pH solution is set to be slightly basic at pH ≈ 9 (pK ≈ 8.3). For the EET acceptor we used dissodium fluorescien (uranin) with its absorption band peak position at 495 nm. We also used Rhodamine 110 as the

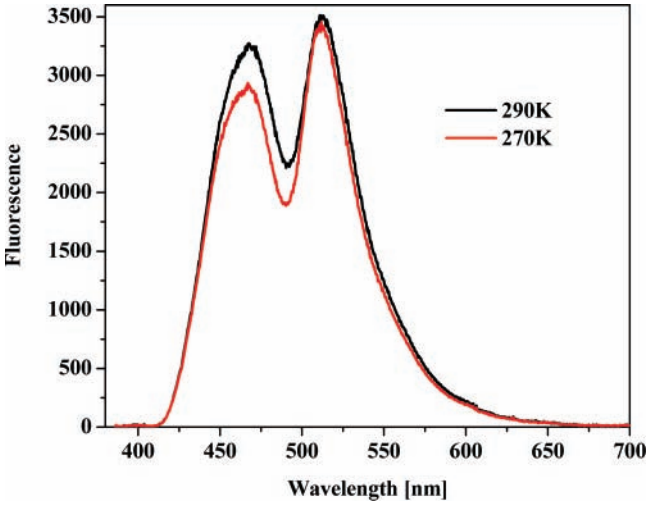

Figure 9. Steady-state emission spectrum of a donor−acceptor system in water and in ice samples.

acceptor. Rhodamine 110 absorption and emission is slightly red-shifted with respect to that of uranin. The excitation processes start with the excitation of the RO^- form of the photoacid at 380 nm ($\epsilon_{380} \cong 1 \times 10^4\ M^{-1}\ cm^{-1}$). The absorption cross section of the uranin acceptor at 380 nm, is only $\epsilon_{380}^{uranine} = 1000\ M^{-1}\ cm^{-1}$. From the overlap of the RO^- emission of 2N68DS with uranin absorption we deduced that the critical EET distance R_0 for RO^- as the donor and uranin as the acceptor is rather large, being $R_0 \cong 55$ Å. The electronic energy transfer rate for 0.3 mM uranin solution is quite efficient and this is clearly seen in Figure 8a, where the intense emission band at 515 nm is composed of the uranin signal emission of about 85%, and only 15% of the emission of the RO^- band. Figure 8b shows the excitation spectra for the emission collected at 540 nm, which is about 25 nm red-shifted from the peak of the strong emission band of uranin. The excitation spectrum clearly shows that the major part of the 515 nm emission is generated by the RO^- excitation at around 380 nm and to a lesser extent by direct excitation of uranin. The similarity between the absorption and the excitation spectra suggests an efficient energy transfer process.

Figure 9 shows the steady-state emission spectra of a liquid and ice samples containing the photoacid and a small concentration of acceptor uranin (about 0.3 mM). The emission spectrum of the sample clearly shows that the uranin emission band at 515 nm is also dominant in the ice phase.

Figure 10 shows the time-resolved emission measured at two wavelength of the ice sample at several temperatures containing both 2N68DS (donor) and uranin (acceptor). The figure shows the time-resolved emission measured at 480 nm (the donor, the RO^- band), and at 540 nm the uranin band. The emission at 540 nm is mainly that of uranin (peak wavelength at 515 nm) with some contribution of the RO^- band of 2N68DS due to band overlaps since the RO^- band peak position is at 475 nm. We observed that the signal rise time at 540 nm attributed to the uranin acceptor emission at high temperatures is about the same in both the liquid and the solid phases at the temperature range $290 > T > 255$ K. We explained that it arises from the efficient EET between the RO^- of 2N68DS and the uranin ($R_0 \simeq 55$ Å).

Figure 11 shows the time-resolved emission of the RO^- band of 2N68DS. The figure shows the signals of two samples, the first sample containing only 2N68DS (no EET process) while the second sample contains also about 0.3 mM uranin. The decay

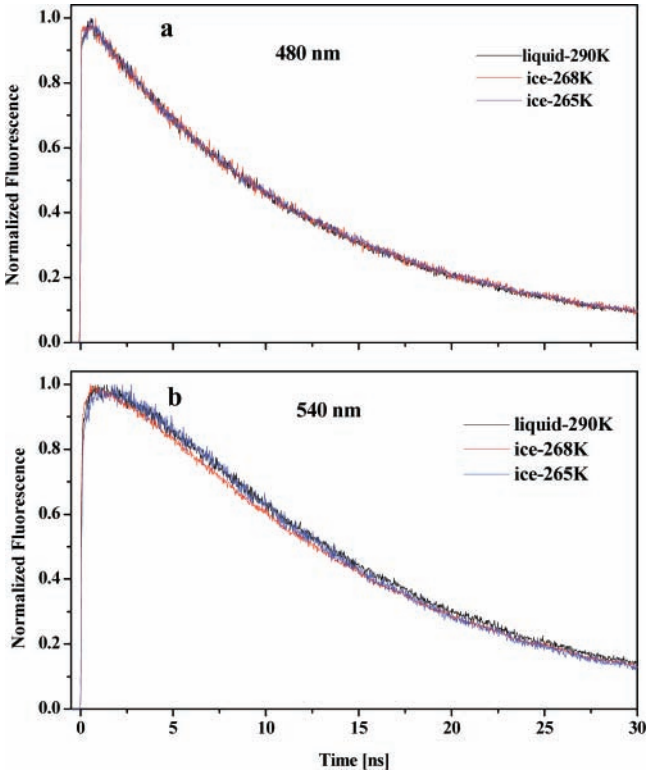

Figure 10. Time-resolved emission at several temperatures of a donor−acceptor system: (a) RO^- band of 2N68DS measured at 480 nm; (b) uranin emission band measured at 540 nm.

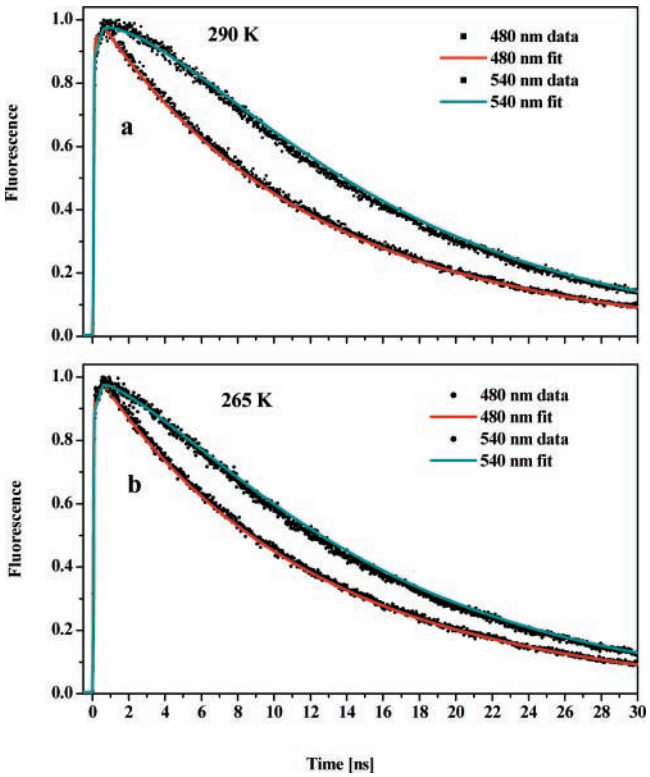

Figure 11. Time-resolved emission at several temperatures of a donor−acceptor sample. The solid curve is a fit using eq 8 (see text) of data shown in Figure 10: (a) RO^- band of 2N68DS measured at 480 nm; (b) uranin emission band measured at 540 nm.

of the sample in the absence of uranin is almost exponential with a lifetime of about 12 ns. As seen in the figure, the signal from the sample where the EET process takes place decays slightly faster at short times whereas at long times the rate is

similar to the sample without uranin and thus the overall signal is nonexponential. We used the EET time dependent equation (eq 8) to fit the experimental signal (solid curve). The equation predicts a square root dependence on time with the EET process taking place in a homogeneous distribution of acceptor molecules in a three-dimensional bulk material.

EET on Hollow Glass Spheres. We used the Förster donor−acceptor electronic energy transfer process to evaluate the distribution of large molecules on polar surfaces. We used for that purpose a commercial micrometer size hollow glass sphere (SiO_2) (Aldrich, CAS 65997) of an average size of 10 μm to mimic the grain boundaries of polycrystalline ice samples. In the case where the photoacid dopants are excluded from the bulk ice upon freezing, it is expected that they will be present at the microcrystal grain boundaries. For these experiments we used 8-hydroxy-1,3,6-pyrenetrisulfonate (HPTS) as the EET donor and rhodamine 110 as the proton acceptor. We coated the glass sphere sample with the donor and acceptor by spraying 50 mg of glass sample with a few drops of methanolic solution ($\sim$30 μL of 10^{-4} M solution) of the two dopants.

Both the donor and the acceptor fluoresce strongly when the glass sample is wet. Dry samples do not fluoresce. We estimate that the fluorescence intensity drops by at least 4 orders of magnitude. We observed similar fluorescence intensity reduction of photoacids when a liquid water photoacid sample froze upon cooling and formed polycrystalline ice.

We interpreted the strong fluorescence reduction in pure ice samples as resulting from the exclusion of the photoacid molecules from the bulk of the microcrystal and their aggregation at the grain boundaries. Dimerization of two photoacid molecules causes the annihilation of the overall transition dipole moment which leads to the reduction in the fluorescence intensity. We found that in order to overcome the aggregation of the photoacid molecules upon sample freezing, it is enough to add to a pure aqueous solution 1% of methanol (by mole ratio). The methanol mediates between the hydrophobic aromatic rings of the photoacid and the ice-water molecules. We found in numerous experiments that the fluorescence intensity of the photoacid in the frozen methanol-doped ice sample is similar to the liquid state.

For further evaluation of the EET process on model surface of microcrystalline ice (hollow glass sphere) we used nonpolar acenes molecules as donor and acceptor. We chose anthracene as the donor and tetracene as the acceptor. The critical radius is rather small $R_0 \approx 26$ Å for this pair. Unlike the polar photoacid uranin pair, both the nonpolar donor and acceptor (anthracene and tetracene) fluoresce on the dry glass spheres.

Parts a and b of Figure 12 show the time-resolved fluorescence of a sample of hollow glass sphere coated with anthracene and tetracene. The sample was excited at 380 nm, the red edge of the anthracene band. Figure 12a shows the emission of the anthracene measured at 430 nm of two samples one with both the donor and the acceptor and a sample where only anthracene is coated on the glass surface. We used the EET process (eq 8) to fit the time-resolved fluorescence of the anthracene in the presence of the tetracene acceptor. The solid line is the computed fit. Figure 12b shows the fluorescence of tetracene on the glass sphere of two samples; the first sample contains both the donor and the acceptor and a sample where the tetracene was directly excited in the absence of anthracene. The solid line in the figure shows the computed fit using eq 8 for the EET process with the same parameters used to fit the donor decay (the anthracene).

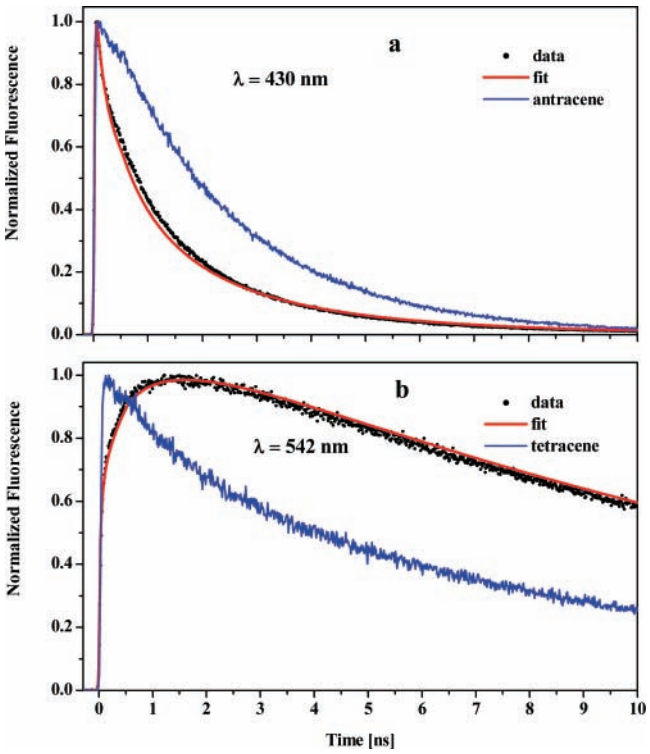

Figure 12. Time-resolved emission of anthracene-tetracene samples coated on hollow glass spheres: (a) emission of the anthracene band (donor), measured at 430 nm along with a fit using eq 8; (b) emission of the tetracene band (acceptor), measured at 540 nm along with calculated fit using eq 8.

Discussion

The main findings of this study are as follows: In ice at the temperature range of 270 K > T > 220 K, the excited-state proton-transfer rate from 2N6S (pK^* $\simeq$ 2.0) is larger in the presence of KF than in the absence of KF. For 2N68DS (a strong photoacid, pK^* $\simeq$ 0.7) the temperature range for the direct proton transfer extends to much lower temperatures, i.e., 270 K > T > 185 K. The change in the time-resolved fluorescence decay curve of the ROH form of a sample in the presence of KF can be fit by an irreversible binary-collison model $L + ROH^* \xrightarrow{k_{PT}^L} LH^+ + RO^{-}{}^*$ where L-defect produced by F^-.

In a previous study we measured the proton transfer in ice and the geminate recombination rates from HPTS and 2N68DS in liquid water and in ice at the high-temperature region of 240 K < T < 270 K containing a small amount of a weak base-like acetate or fluoride.[26] We found that both the acetate and the fluoride anions can react with a proton that was first transferred to the liquid water or to ice by an excited photoacid. The proton in ice diffuses and may react with the weak base in the ice. It was found that the proton scavenging effect in ice is much larger than that in the liquid state. Below, we briefly describe the model of a reversible photoprotolytic cycle of a photoacid that also accounts for the proton scavenging in the ice by F^- ions.

Reversible Diffusion-Influenced Two Step Proton-Transfer Model with Inclusion of a Proton Scavenger in Solution. In this model,[11,29,30] the photoprotolytic cycle in the excited-state is subdivided into the two consecutive steps of reaction and diffusion. The mathematical and computational details are given elsewhere.[30,31] It is based on solving of the Debye−Smoluchowski equation (DSE) coupled to an ordinary chemical

kinetic equation. The emitted proton, while diffusing in liquid solution or in ice may react with a mild base like acetate or fluoride anion. The reaction is easily observed as a strong reduction of the intensity of the ROH long time fluorescence tail.

To account for the proton reaction with the base anion we introduced a special bimolecular reaction term.[26] The negatively charged F^- is not evenly distributed around the negatively charged photoacid molecule in the ground electronic state. As a consequence we used the Debye−Hückel screened Coulomb potential[12] to account for the presence of KF in ice.

Direct Proton Transfer from an Excited Photoacid to Ice in the Presence of a Fluoride Ion. We propose that in the presence of F^- in methanol-doped ice, a direct proton transfer occurs from the excited photoacid to a mobile L-defect created by a fluoride. The fluoride ion creates a mobile L-defect that is capable of reacting with an excited photoacid. L-defect mobility exhibits a low activation energy,[32] and it is thus able to approach the excited photoacid, even at very low temperatures.

The electrical properties of ice are sensitive to small concentrations of certain impurities that can be incorporated into the hydrogen-bonded network to generate a point defect. HF is the classical example. An HF molecule is substituted to an H_2O molecule in an ice hexagonal structure, leaving one bond which lacks a proton. A rotation of an H_2O molecule next to it adds a proton on this bond and an L-defect is released into the ice.[18] L-defects are mobile and react with H_3O^+ and probably with strong and mild acids or acidic sites in ice. The literature value of the mobility activation energy ranges from 0.23 eV[18] to almost zero.[32] The value of the mobility of an L-defect at 218 K is 2.5×10^{-9} m^2 V^{-1} $s^{-1}$and compares to a high-temperature proton mobility at 263 K 2.8×10^{-8} m^2 V^{-1} s^{-1}.[18]

There are two reactions of L-defects that take place in doped ice with photoacid molecules:

The first reaction of the L-defect is when the proton is released from the excited photoacid to the ice structure by a laser light pulse. At first the proton is transferred to nearby water molecules surrounding the photoacid. The second step is proton diffusion in the ice crystal. The proton may react with an L-defect created by F^- or recombine geminately with the RO^- form of the photoacid to reproduce the ROH* that can start another photocycle. Since the L-defect is mobile the proton scavenging process is more efficient than the static F^- reacting with the mobile proton. If the scavenging reaction rate is diffusion-controlled then the reaction rate is determined by the mutual diffusion constant $D = D_{H+} + D_L$. The diffusion constant of an L-defect in ice is of the same proton order and hence the proton scavenging rate constant is larger by about a factor of 2. This evidence can explain the large scavenging rate in ice, which was found to be larger than in liquid water from our previous study.

The second reaction of the L-defect in F^- doped ice is a direct proton transfer from the excited photoacid itself. At sufficiently low temperatures in methanol-doped ice, the conventional proton-transfer rate from an excited-state photoacid to H_2O is much slower than at the highest ice temperature of $T \approx 270$ K. At about 240 K the proton-transfer rate constant from 2N68DS to ice is about 10^9 s^{-1} compared to about 7×10^9 s^{-1} at 270 K. At such a low rate constant (time constant of ~1 ns) the L-defect mobility is sufficiently large enough to enable even the small concentration of L-defect (created by a few mM F^- ions) to reach the protonated photoacid within the excited-state lifetime. The proton is being transferred directly from the photoacid to the L-defect. Such a scenario occurs efficiently in 20 mM F^- doped ice at the temperature range of 240 K < T < 185 K. In the past[35] in liquid solution we used a model to describe the direct reaction of a base molecule at a large concentration of c > 0.5 M with an excited photoacid molecule. Such a reaction is similar to the reaction occurring between an excited-state photoacid and an L-defect created by F^- ions incorporated at a lattice site of hexagonal ice. Below, we briefly describe the model. A more detailed description is given in ref 31 and references therein.

The Smoluchowski Model. The mathematical and computational details of the Smoluchowski model are given elsewhere.[33] According to the Smoluchowski model, the survival probability of a single (static) donor (here, ROH*) due to its irreversible reaction with a $c = [B^-]$ concentration of proton acceptors (in this study L-defect) is given by[34−36]

$$S(t) = \exp(- c \int_0^t k(t')\, dt') \tag{9}$$

where $k(t)$ is the time-dependent rate coefficient for the donor−acceptor pair

$$k(t) = k_{PT} p(a,t) \tag{10}$$

whose proton-transfer rate constant is k_{PT}. The pair (ROH*/B^-) density distribution, $p(r,t)$, is governed by a Smoluchowski equation [diffusion in a potential $U(r)$] in three dimensions.[37]

We solved the Smoluchowski equation numerically, using a user-friendly Windows application for spherically-symmetric diffusion problems (SSDP, version 2.61)[38] to yield $k(t)$ in eq 9.

For $U(r) = 0$, it is possible to solve the above equations analytically for $k(t)$.[35] This is no longer true when $U(r) \neq 0$. In this case, Szabo[36] found an approximate expression for the time-dependent rate constant:

$$k(t) = \frac{4\pi D a_e k_{PT} e^{-\beta U(a)}}{k_{PT} e^{-\beta U(a)} + 4\pi D a_e} \left\{ 1 + \frac{k_{PT} e^{-\beta U(a)}}{4\pi D a_e} e^{\gamma^2 D t} \mathrm{erfc}[(\gamma^2 D t)^{1/2}] \right\} \tag{11}$$

where γ is given by

$$\gamma = a_e^{-1} \left(1 + \frac{k_{PT} e^{-\beta U(a)}}{4\pi D a_e} \right) \tag{12}$$

erfc is the complementary error function and a_e is an effective radius.

Equation 11 is exact when the potential is zero, i.e., $U = 0$ and $a_e = a$. When a potential is introduced, it behaves correctly at both t=0 and t=∞

$$k(0) = k_{PT} e^{-\beta U(a)}, \quad k(\infty) = [k(0)^{-1} + k_D^{-1}]^{-1} \tag{13}$$

where $k_D = 4\pi D a_e$ is the diffusion-control rate constant. The nonexponentiality in $S(t)$ is a result of a time-dependent rate constant $k(t)$, as depicted by the ratio

$$k(0)/k(\infty) = 1 + k(0)/k_D = \gamma a_e$$

From the time-dependent rate constant, $k(t)$, one can calculate the survival probability of an ROH* molecule surrounded by an equilibrium distribution of ions. To account for the conventional ESPT process and the pure radiative lifetime of ROH, which occurs in parallel and supposedly independently from the reaction in eq 9, we write

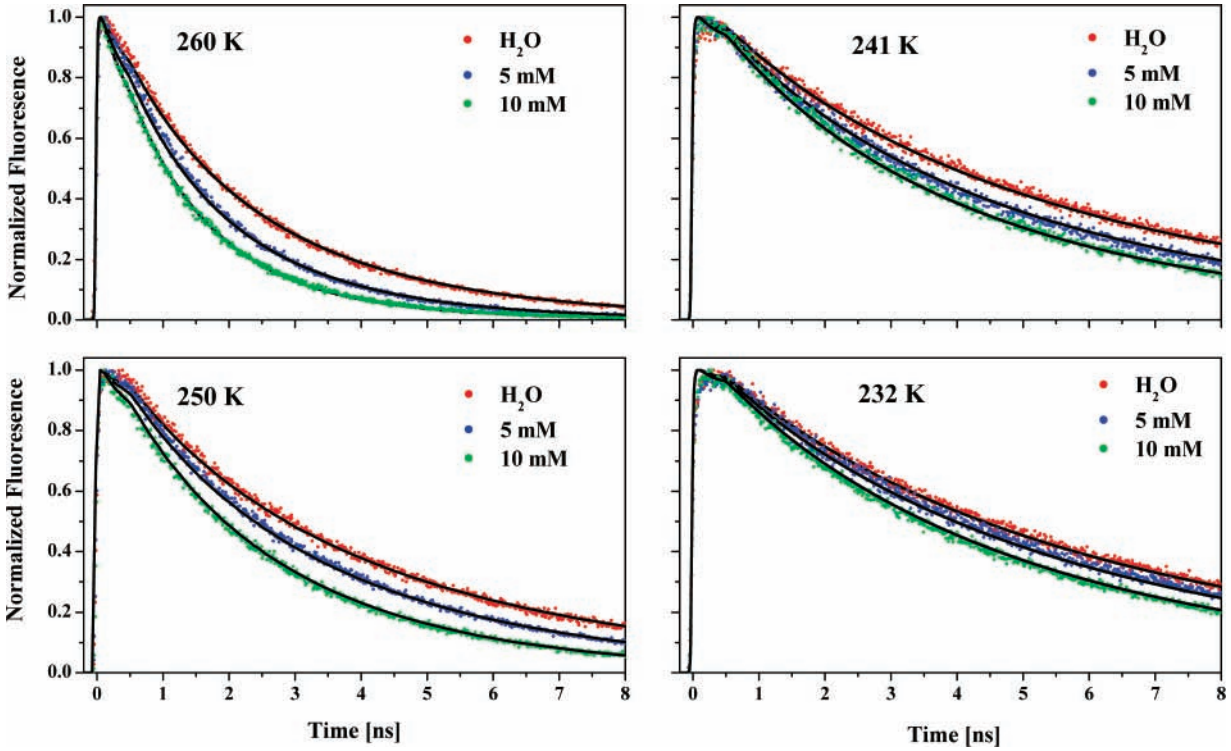

Figure 13. Time-resolved emission of the ROH* band of 2N6S measured at several temperatures along with computer fits: (dots) experimental data; (solid line) calculated fit using our model.

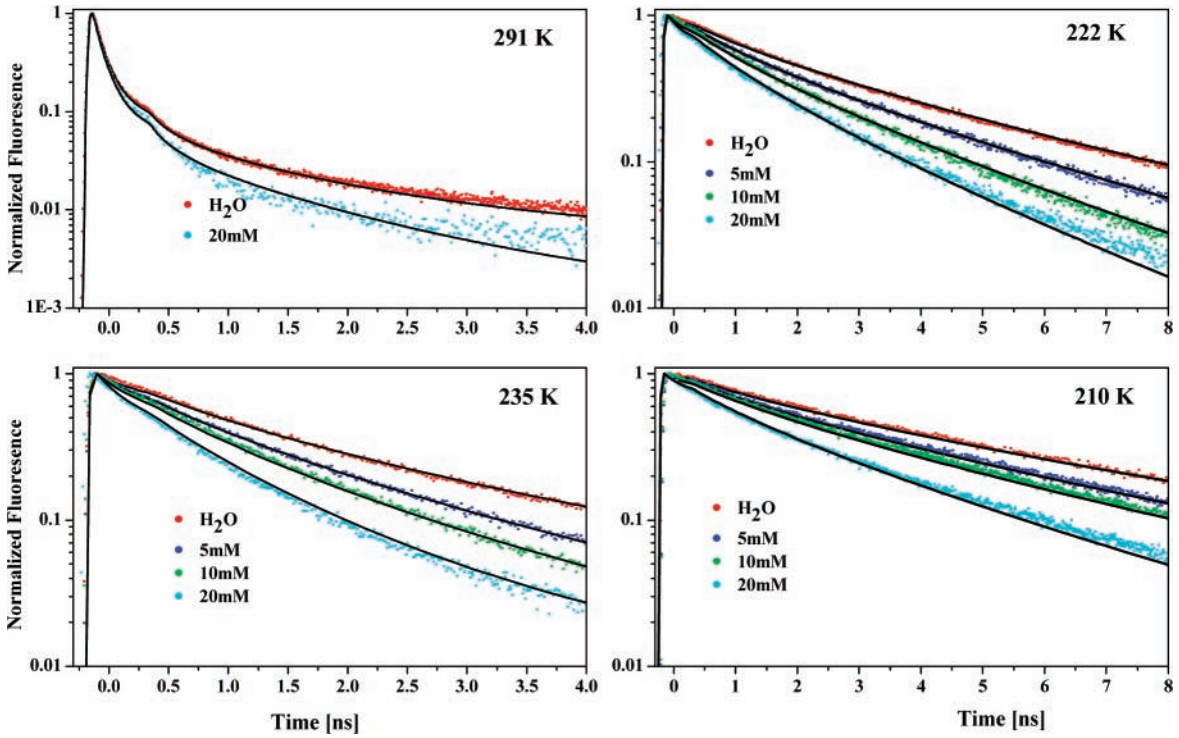

Figure 14. Time-resolved emission of the ROH* band of 2N68DS measured at several temperatures along with computer fits: (dots) experimental data; (solid line) calculated fit using our model.

$$S'(t) = \exp(-t/\tau - c\int_0^t k(t')\,dt') \qquad (14)$$

where $1/\tau = 1/\tau_{rad} + 1/\tau'_{PT}$, $1/\tau'_{PT}$ is the proton transfer rate to ice in the absence of F^-. This quantity, with an independently measured τ (in the absence of KF), is used in comparison with the experimental signal.

Model Fitting the Experimental Results. Figure 13 shows both the model fitting (solid curves) and the experimental results (dots) of the ROH emission of 2N6S in ice containing 5 and 10 mM of KF at several temperatures (see Figure 1). The fitting is rather good at all temperatures and at concentrations of both 5 and 10 mM KF.

TABLE 1: Fitting Parameters for the Diffusion Influenced Irreversible Binary Reaction Model of 2N6S with KF

T [K]	k_{PT}^{L} [10^9 Å s^{-1}]	D [cm^2 s^{-1}][a,b]
260	14	4×10^{-5}
241	3	1×10^{-5}
232	1.8	7×10^{-6}
222	1.5	5×10^{-6}
210	0.8	4×10^{-6}

[a] Contact radius $a = 8$ Å. [b] Effective L-defect concentration $c_{eff} = 2.5\ c_{KF}$.

TABLE 2: Fitting Parameters for the Diffusion Influenced Irreversible Binary Reaction Model of 2N68DS with KF

T [K]	D [cm^2 s^{-1}][a,b,c]
260	4×10^{-5}
241	1.2×10^{-5}
235	6.5×10^{-6}
222	4.5×10^{-6}
210	2.5×10^{-6}
197	7×10^{-7}

[a] Contact radius $a = 8$ Å. [b] Effective L-defect concentration $c_{eff} = 2.5\ c_{KF}$. [c] Reaction rate constant $k_{PT}^{L} = 100$ [10^9 Å s^{-1}].

Figure 14 shows the model fitting of the time-resolved emission of the ROH form of 2N68DS in methanol-doped ice in the presence of 5, 10, and 20 mM KF at several temperatures (see Figure 2). We used the model described above to account for the reaction

$$L + ROH^* \xrightarrow{k_{PT}^{L}} LH^+ + RO^-* \qquad (15)$$

The ROH* hydroxyl proton is transferred directly to a mobile L-defect that was created by F^- in ice. This reaction depends on several parameters. The parameters used in our model are the concentration of the L-defect c_L, the diffusion constant of the L-defect D_L, the intrinsic reaction rate constant k_{PT}^{L}, and the contact radius of the reaction sphere a_L. In addition to the parameters mentioned above, we have to take into account the Debye−Hückel screening, which is due to the presence of KF in ice of the Coulomb potential and the effective charge of an L-defect−0.38e, where e is the electronic charge.

We got a good fit to the experimental results using the parameters given in Tables 1 and 2. At the contact sphere, the reaction rate constant k_{PT}^{L} for 2N68DS is about 100 Å/ns. The accurate value of the intrinsic rate constant k_{PT}^{L} at various temperatures in the range of $200 < T < 270$ K cannot be determined when the concentration of F^- ions is small, i.e., $c_{F^-} \leq 20$ mM, and the diffusion-controlled rate constant k_D is smaller than k_{PT}^{L}. In such a case the rate-limiting step is the transport of the L-defect toward the photoacid (see eq 9). When we used values for $k_{PT} \geq 100$ Å/ns we were unable to find differences in the fit to the data in ice in the range $200 < T < 270$ K. In our previous studies we got a very large rate constant in liquid water using large concentration of acetate base ($c > 0.5$ M) which reacts directly with HPTS ROH ($k = 150$ Å/ns). Mohammed et al.[39] found a similar rate constant for the reaction between excited HPTS and the concentrated solution of acetate, $c > 1$ M, which forms a "loose complex" already in the ground-state.

At 220 K the diffusion constant of the L-defects in ice is 2.5×10^{-6} cm^2/s. This value is close to the one calculated from the Einstein−Stokes relation published mobility value of 2.5×10^{-9} m^2 V^{-1} s^{-1} at 218 K. For a good fit we had to compromise on the value of the L-defects' local concentration c_L. The effective L-defect concentration we used in the fit is about 2.5 times larger than the actual KF concentration. The concentration enters the calculations in eq 14 and it basically affects the diffusion-time to reach the reaction sphere. The larger the concentration, the smaller the number of steps the random walker that placed at the average distance of an L-defect from the photoacid needs in order to reach the reaction sphere. The larger effective concentration of the L-defect may indicate that the L-defect motion is not only a pure random walk of short distance steps but also exhibits some longer jumps. According to molecular dynamic simulations[23] in ice, the defect motion cannot be described as random diffusion between all available sites, preferred sites, performing excursions around these sites. The time spent at the "trap sites" is typically several picoseconds, but it may be as long as a few tens of picoseconds.[23] In the current study, we also found that it is necessary to use a rather larger contact radius $a = 8$ Å to obtain a good fit at all times. In previous studies in the liquid-state we used $a = 7$ Å, the same value that Weller[3] used for the contact radius of the acetate reaction with a photoacid. The larger value for the contact sphere radius supports the results of Buch's simulation of L-defect motion in the preferred path in ice.[23] It can also fit the picture that the proton-transfer reaction does not occur at a contact point between an L-defect and the hydroxyl group of the photoacid but rather the proton jumps a longer distance to the L-defect. The proton jumps to the L-defect via a bridge of one or two water molecules. This picture has some similarity with Mohammed et al.,[39] "loose complex" proton-transfer mechanism.

We used similar values of the L-defect diffusion constant D_L for the fit of the luminescence signal of the ROH of both 2N6S and 2N68DS. The values of the intrinsic reaction rate k_{PT}^{L}, obtained from the best fitting of the experimental data of 2N6S, are much smaller than for 2N68DS. The values for the reaction of L-defect with ROH range from $k_{PT}^{L} = 14$ Å/ns at 260 K down to $k_{PT}^{L} = 0.8$ Å/ns at 210 K. When compared with the regular ESPT rate constant of 2N68DS ($pK^* = 0.7$) in both water and ice the small values of k_{PT}^{L} obtained for 2N6S ($pK^* = 2$) are in accord with the smaller photoacidity that is more than 1 order of magnitude smaller than 2N68DS. Comparison of the fitting values of k_{PT}^{L} of 2N68DS with those of 2N6S shows that the ratio between rate constants of direct proton transfer to an L-defect is a similar to the ratio for the regular ESPT process between the two photoacids.

Summary

We studied the photoprotolytic cycle of two excited photoacids, 2N6S and 2N68DS, in methanol-doped ice in the presence of a low concentration of a weak-base like F^-. According to models, when an HF molecule is substituted with an H_2O molecule in an ice hexagonal structure, it creates one bond which lacks a proton. A rotation of an H_2O molecule next to it adds a proton to this bond and an L-defect is released into the ice.[18] We propose that the fluoride ion creates a mobile L-defect capable of reacting with an excited photoacid. We found that at temperatures of $200\ K < T < 270$ K the effective decay rate of ROH, the protonated form of the photoacid, depends on the fluoride concentration. The rate increased as the fluoride concentration increased. The rise rate of the RO^- emission signal showed a complementary response. The rise-time decreased as the fluoride concentration increased. The increase in the proton-transfer rate in the presence of KF is explained by the assumption that in addition to the proton transfer to the solvent, a direct proton transfer occurs from the excited photoacid to a mobile L-defect created by a fluoride ion. L-defect mobility

exhibits a low activation energy,[32] and can thus approach the excited photoacid, even at very low temperatures. We used a model of diffusion influenced irreversible binary reaction based on the Smoluchowski equation to quantitatively fit the time-resolved emission data of the ROH in the presence of F^- ion in ice.

The data fit showed a linear dependence of the effective concentration of the L-defect on the F^- concentration. The diffusion constant of the L-defect is large and is comparable to that of proton in ice. At $T \approx 260$ K, $D \approx 4 \times 10^{-5}$ cm^2/s while its value at about 200 K is $D \approx 4 \times 10^{-6}$ cm^2/s. The intrinsic reaction rate of L-defect with the photoacid depends on the strength of the photoacid. For a strong photoacid like 2N68DS (p$K^* = 0.7$) we found a value of $k_{PT}^{L} \geq 100$ Å/ns at all temperatures. For a weak photoacid 2N6S (p$K^* = 2$) we found that $k_{PT}^{L} \geq 10$ Å/ns at 260 K and 1 Å/ns at 210 K.

In this study we also characterized the polycrystalline ice samples. We used time-resolved and steady-state emission techniques to measure the EET from an excited donor molecule to an acceptor in methanol-doped ice. The results indicate that only a mild change in the EET rate and its efficiency occurs when a liquid aqueous solution freezes. If upon sample freezing the donor and acceptor molecules tend to be excluded out of the ice crystal bulk and are concentrated at the grain boundaries, the EET process will be much more efficient in frozen samples than in liquid samples. For a 1 mM acceptor concentration and microcrystals of the size of 10 μm (poly crystalline ice), the average distance between molecules is 5 Å at the grain boundaries whereas in the bulk the average distance is close to 100 Å. The EET process is sensitive to the distance between an excited donor and an acceptor. The donor−acceptor pair we used has a rather large critical radius R_0 for EET and hence can easily monitor the large difference between a sample that consists of a homogeneous distribution of photoacids or uranin molecules in frozen polycrystalline ice or a samples in which the donors and/or the acceptors are only present at the grain boundaries.

Acknowledgment. We thank Prof. V. Buch and Dr. H. Diamant for their helpful and fruitful suggestions and discussions. This work was supported by grants from the Binational US−Israel Science Foundation and the James-Franck German-Israel Program in Laser-Matter Interaction.

References and Notes

(1) Bell, R. P. *The Proton in Chemistry*, 2nd ed.; Chapman and Hall: London, 1973.
(2) *Proton Transfer Reaction*; Caldin, E. F., Gold, V., Eds.; Chapman and Hall: London, 1975.
(3) (a) Weller, A. *Prog. React. Kinet.*, **1961**, *1*, 189. (b) *Z. Phys. Chem. N. F.* **1958**, *17*, 224.
(4) Ireland, J. E.; Wyatt, P. A. *Adv. Phys. Org. Chem.* **1976**, *12*, 131.
(5) (a) Gutman, M.; Nachliel, E. *Biochim. Biophys. Acta*, **1990**, *391*, 1015. (b) Pines, E.; Huppert, D. *J. Phys. Chem.* **1983**, *87*, 4471.
(6) Kosower, E. M.; Huppert, D. *Annu. Rev. Phys. Chem.* **1986**, *37*, 127.
(7) Tolbert, L. M.; Solntsev, K. M. *Acc. Chem. Res.*, **2002**, *35*, 1.
(8) Rini, M.; Magnes, B. Z.; Pines, E.; Nibbering, T. J. *Science* **2003**, *301*, 349.
(9) Prayer, C.; Gustavsson, T.; Tarn-Thi, T. H. *Fast Elementary Processes in Chemical and Biological Systems*, *54th International Meeting of Physical Chemistry*; AIP: New York, 1996; p 333.
(10) Tran-Thi, T. H.; Gustavsson, T.; Prayer, C.; Pommeret, S.; Hynes, J. T. *Chem. Phys. Lett.* **2000**, *329*, 421.
(11) Agmon, N. *J. Phys. Chem. A*, **2005**, *109*, 13.
(12) Leiderman, P.; Gepshtein, R.; Uritski, A.; Genosar, L.; Huppert, D. *J. Phys. Chem. A* **2006**, *110*, 9039.
(13) Leiderman, P.; Gepshtein, R.; Uritski, A.; Genosar, L.; Huppert, D. *J. Phys. Chem. A* **2006**, *110*, 5573.
(14) Uritski, A.; Leiderman, P.; Huppert, D. *J. Phys. Chem. A* **2006**, *110*, 13686.
(15) Fletcher, N. H. *The Chemical Physics and of Ice*; Cambridge University Press: London, 1970; Chapter 9.
(16) Hobbs. P. V. *Ice Physics*; Clarendon Press: Oxford. U.K., 1974; Chapter 2.
(17) Von Hippel, A.; Runck, A. H.; Westphal, W. B. In *Physics and Chemistry of Ice*; Walley, E., Jones, S. J., Gold, L. W., Eds.; Royal Society of Canada: Ottawa, 1973; p 236.
(18) Petrenko, V. F.; Whitworth, R. W. *The Physics of Ice*; Oxford University, Press: Oxford, U.K., 1999.
(19) Kelly, I. J.; Salomon, R. R. *J. Phys. Chem.* **1969**, *50*, 75.
(20) Jaccard, C. *Ann. N.Y. Acad. Sci.* **1965**, *125*, 390−400.
(21) Bjerrum, N. *Science* **1952**, *115*, 385.
(22) Kobayashi, C.; Saito, S.; Ohmine; I. *J. Chem. Phys.* **2001**, *115*, 4742.
(23) Podeszwa, R.; Buch, V. *Phys. Rev. Lett.* **1999**, *83*, 4570.
(24) Takenaka, N.; Tanaka, M.; Okitsu, K.; Bandow, H. *J. Phys. Chem. A* **2006**, *110*, 10628.
(25) Heger, D.; Klanova, J.; Klan, P. *J. Phys. Chem. B* **2006**, *110*, 1277.
(26) Uritski, A.; Leiderman, P.; Huppert, D. *J. Phys. Chem. C* **2007**, *111*, 8856.
(27) Leiderman, P.; Uritski, A.; Huppert, D. *J. Phys. Chem.* **2007**, *111*, 4998.
(28) Förster, Th. *Ann. Phys. Ser. 6* **1948**, *2*, 55.
(29) Pines, E.; Huppert, D. *J. Chem. Phys.* **1986**, *84*, 3576.
(30) Pines, E.; Huppert, D.; Agmon, N. *J. Chem. Phys.* **1988**, *88*, 5620.
(31) Agmon, N.; Pines, E.; Huppert, D. *J. Chem. Phys.* **1988**, *88*, 5631.
(32) Kunst, M.; Warman, J. M. *J. Phys. Chem.* **1983**, *87*, 4093.
(33) Cohen, B.; Huppert, D.; Agmon, N. *J. Phys. Chem. A* **2001**, *105*, 7165.
(34) Von Smoluchowski, M. *Z. Phys. Chem.* **1917**, *92*, 129.
(35) Tachiya, M. *Radiat. Phys. Chem.* **1983**, *21*, 167.
(36) Szabo, A. *J. Phys. Chem.* **1989**, *93*, 6929.
(37) Rice, S. A. In *Comprehensive Chemical Kinetics*; Bamford, C. H., Tipper, C. F. H., Compton, R. G., Eds.; Elsevier: Amsterdam, 1985; Vol. 25.
(38) Krissinel', E. B.; Agmon, N. *J. Comput. Chem.* **1996**, *17*, 1085.
(39) Mohammed, O. F.; Pines, D.; Dreyer, J.; Pines, E.; Nibbering, E. T. J. *Science* **2005**, *310*, 5745.